Chemical Science

ROYAL SOCIETY OF CHEMISTRY

EDGE ARTICLE

View Article Online
View Journal | View Issue

Cite this: *Chem. Sci.*, 2025, **16**, 18928

All publication charges for this article have been paid for by the Royal Society of Chemistry

Received 22nd June 2025
Accepted 9th September 2025

DOI: 10.1039/d5sc04587h

rsc.li/chemical-science

Matere bond identification in non-crystalline materials by using X-ray photoelectron spectroscopy

Oleg Semyonov,[a] Nikita S. Antonkin,[a] Amirbek D. Radzhabov,[a] Andrea Pizzi, *[b] Cristina Lo Iacono,[b] Olga Guselnikova,[ac] Sergi Burguera,[d] Antonio Frontera, *[d] Giuseppe Resnati *[ab] and Pavel S. Postnikov *[a]

The Re atoms in perrhenate salts can act as electrophiles and form, with nucleophiles, adducts assembled *via* Re···O interactions. X-ray photoelectron spectroscopy (XPS) is proven here as a reliable technique to identify the presence of such interactions (commonly named matere bonds, MaBs) in powders. Specifically, ten hybrid organic–inorganic perrhenate salts are described and their single crystal X-ray (XRD) analyses allowed for establishing that short σ-hole Re···O MaBs were present in seven of them. The Re $4f_{7/2}$ photoelectron energy is smaller in these systems than in those wherein the interaction is absent. This signal is thus a valuable tool to identify the MaB presence in non-crystalline samples, namely XPS complements single crystal X-ray analyses in determining the MaB presence.

Introduction

Non-covalent interactions involving σ-holes[1,2] play an important role in numerous biological[3] and chemical (catalysis, sorption, *etc.*)[4–7] phenomena and their investigation is instrumental in understanding molecular recognition and self-assembly processes.[8,9] For instance, the halogen bonding (HaB),[10] the best known σ-hole interaction and the first one to be given an IUPAC definition,[11] can remarkably contribute to the binding affinity, selectivity, and pharmacological properties of drugs.[12–15] HaBs have been exploited in the design of catalysts and sorbents with tailored properties, including increased selectivity, reactivity, and stability.[16–18] Moreover, the HaB enables assembling ordered layers in crystalline materials and enhancing the performance and long-term stability of photovoltaic devices.[19–21]

In addition to halogens, other p-block elements such as chalcogens,[22] pnictogens,[23] tetrels,[24–26] and triels[27] (*i.e.*, elements of groups 16, 15, 14, and 13, respectively) can form σ-hole bonds[28] and the same holds for various elements of the d-block.[29–37] Recently, it has been shown that all three group 7 elements can function as electrophilic sites[38] and the term matere bond (MaB) has been introduced to designate these non-covalent interactions. The MaB has been proved to drive the formation of adducts not only between neutral compounds,[39] but also between anions.[40] Perrhenate, pertechnetate, and permanganate anions form anion···anion adducts with quite different topologies, for instance, discrete adducts as well as 1D and 2D networks. Indeed, the utilization of d-group metals as σ-hole donors seems to receive rapidly increasing attention in the scientific community.[41] These metals possess unique electronic configurations, allowing them to exhibit diverse coordination geometries and oxidation states and to participate in a range of non-covalent interactions, depending on the specific ligands and the coordination environment.[42,43] This versatility enables the formation of a kaleidoscopic diversity of metal-complexes and metal–organic frameworks and provides opportunities for tailored design and control over molecular recognition and assembly processes. Non-covalent interaction in d-group metals can influence their well-known catalytic efficiency for a wide range of reactions,[34,44] and the same holds for sensing and drug delivery.[40]

Extensive experimental and computational studies on different non-covalent interactions are needed to understand and rationalize their basic aspects in view of applications. Single crystal X-ray diffraction (SCXRD) is a powerful technique to prove unambiguously the presence of a non-covalent interactions. However, growing suitable crystals is often a non-trivial challenge.

X-ray photoelectron spectroscopy (XPS) is a powerful tool to identify different chemical states of compounds. For example, Baines *et al.* employed XPS for the determination of gallium oxidation state in ambiguous complexes for valuable insight

[a]*Research School of Chemistry and Applied Biomedical Sciences, Tomsk Polytechnic University, Tomsk 6340034, Russian Federation. E-mail: pavelpostnikov@gmail.com*

[b]*NFMLab, Department of Chemistry, Materials and Chemical Engineering "Giulio Natta", Politecnico di Milano, I-20131 Milano, Italy. E-mail: andrea.pizzi@polimi.it; giuseppe.resnati@polimi.it*

[c]*Vienna University of Technology, Institute of Applied Physics, Karlsplatz 13, 1040 Vienna, Austria*

[d]*Department of Chemistry, Universitat de les Illes Balears, Crta. de Valldemossa, 07122 Palma de Mallorca, Baleares, Spain. E-mail: toni.frontera@uib.es*

into reactivity.[45] Fantauzzi *et al.* succeeded in the identification of sulfides and polysulfides by XPS.[46] Moreover, XPS can be applied also for determining non-covalent interactions. Indeed, it has been demonstrated by Schroeder's group that XPS spectroscopy can distinguish between ionic salts and neutral cocrystals, and can even identify quasi-symmetrical hydrogen bonds.[47–49] Nangia's group mapped the salt–cocrystal continuum in various pyridine compounds.[50]

In addition, XPS was applied to corroborate the presence of halogen bonded compounds.[18,19,51] To the best of our knowledge, there are no previous reports on XPS studies aimed at identifying any other σ-hole interaction, MaB included. Solid-state NMR spectroscopy[52,53] allows for detecting the MaB presence, but ultrahigh fields are required and single crystal analyses remains the by far most used technique to identify the interaction. It is therefore of interest to find out new techniques to assess the presence of MaB also when no single crystal is available. Possibly the technique should also give information on geometric or energetic features of the bonding. Herein we report a small library of perrhenate salts that was characterized through single crystal XRD to check the presence/absence of MaBs. Then the same samples have been analyzed through XPS in order to determine the differences in the photoelectron energy of Re 4f signals between systems wherein the interaction is present and absent. This energy is smaller in the salts that are matere-bonded than in those that are not. Importantly, a good correlation was found between the interaction length and the binding energy (BE) so that XPS is proven as a reliable and particularly valuable technique to identify MaBs even in non-crystalline samples.

Results and discussion

The presence of some σ-hole interactions, such as halogen or chalcogen bondings, is associated with shifts and/or appearance of new signals in UV-visible, IR, and Raman spectra.[54] More pertinent, σ-hole bonds formation causes shifts also of XPS signals and this is the case for 3d signals of iodine when iodocarbons act as halogen bond donors.[18] For this reason, we expected that XPS could be used as a reliable and unambiguous technique to detect MaB presence. We synthesized several perrhenate salts (Fig. 1) and we characterized them through single crystal X-ray diffraction in order to unambiguously establish the presence (salts **1a–g**) or absence (salts **2a–c**) of MaBs. The purity of all synthesized compounds was evaluated by comparing simulated and experimental powder X-ray patterns (see SI). To maximize our understanding of the relationship between MaB presence/absence and XPS data, hybrid organic–inorganic salts with a diverse assortment of cations were prepared and $AgReO_4$ (**1h**) was studied in order to consider also inorganic salts. This approach aimed at gathering information on the variations in the BE exhibited by photoelectron signals of Re atoms of perrhenate anions experiencing different chemical environment, namely different interactions patterns with the objective to identify the specific BEs variations related to MaB presence.

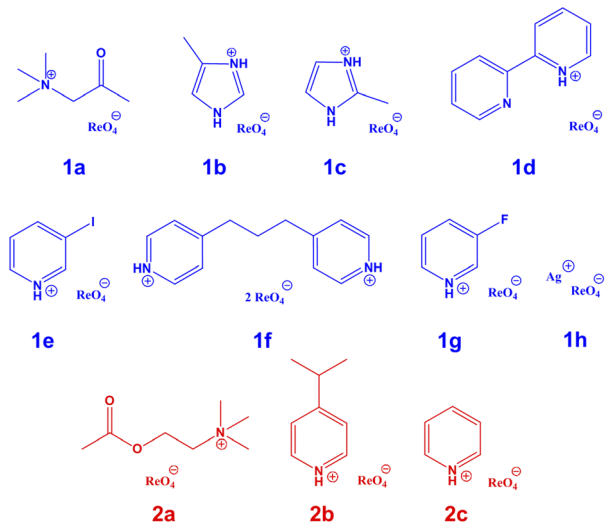

Fig. 1 Structural formulae of the perrhenate salts with (in blue) and without (in red) MaB.

Perrhenate salts **1a–g** display short Re···O contacts, leading to different supramolecular assemblies (Fig. 2). The Re···O separations and the O–Re···O angles (Table 1) allow for rationalizing these interactions as MaBs.

In detail, salt **1a**, recently reported by some of us,[38] shows a cation–anion dimer where the carboxylic –OH of betaine is functioning as a nucleophile towards the Re atom of the perrhenate anion and a Re···O MaB is formed on the extension of one of O–Re perrhenate bonds. This dimer is stabilized also by a hydrogen bond (HB) involving another oxygen of the anion and the $-CH_2$ moiety of betaine cation.

In salts **1b–g** the MaBs assembles anion···anion adducts whose formation is probably favored by the presence of a network of HBs between anions and cations.[55]

Salts **1b,c** (ref. 32) and **1f** form anion infinite chains where each ReO_4^- units function as electrophile (MaB donor) *via* the rhenium atom and nucleophile (MaB acceptor) *via* one of the oxygen atoms.

Salts **1d,e** form anion···anion dimers *via* the antiparallel pairing of two anion units. Similar to the infinite chains formed

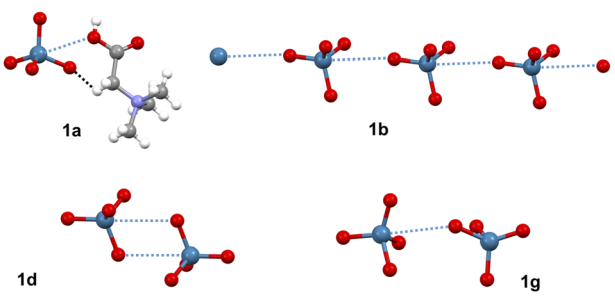

Fig. 2 Ball and stick representation of the supramolecular assemblies formed by MaB in salts **1a**, **1b**, **1d**, and **1g**. Compounds **1c** and **1f** afford anion···anion infinite chains similar to those of **1b**; compound **1e** affords dimers similar to those of **1d**. Color code: navy, rhenium; red, oxygen; grey, carbon; whitish, hydrogen; indigo, nitrogen.

Table 1 Geometric parameters of the MaBs observed in salts **1a–h**

Perrhenate salt	Nc[a]	Re···O distance (Å)	O–Re···O angle (°)	MaB type and topology in obtained adducts
1a	0.925	3.329	177.09	Anion–cation dimer
1b	0.959	3.454	171.11	Anion infinite chain
1c	0.956	3.441	172.66	Anion infinite chain
1d	0.957	3.445	176.21	Anion antiparallel dimer
1e	0.942	3.392	176.45	Anion antiparallel dimer
1f	0.880	3.168	176.97	Anion infinite chain
1g	1.03	3.717	156.46	Anion dimer
1h	0.848	3.052	174.03	Anion antiparallel dimer

[a] The "Normalized contact" Nc for an interaction involving atoms i and j is the ratio D_{ij}/(RvdW,i + RvdW,j) where D_{ij} is the experimental distance between i and j and RvdW,i and RvdW,j are the van der Waals radii of i and j.

by **1b,c,f**, any anion acts both as donor and acceptor of electron density, but in **1d,e** dimers the interacting units are doubly pinned to each other by two MaBs. In the inorganic salt **1h** anions self-assemble *via* antiparallel pairings of Re–O moieties similar to those observed in **1d,e**; any anion forms four such supramolecular synthons and an adamantanoid infinite network is assembled.

Crystals of **1g** displays singly pinned anion···anion dimers, where one ReO_4^- act as MaB donor and the other one as MaB acceptor. Although in this last case the Re···O distance is close to the sum of the van der Waals radii of the involved elements, the O–Re···O angle (156.46°) allows to rationalize it as a MaB.

Perrhenate salts **2a** and **2c** have been previously reported[52,56] and along with the newly prepared salt **2b** they have been used as control samples wherein no Re···O interaction is present, *i.e.*, their X-ray photoelectron spectra have been studied in comparison to those of **1a–h** in order to assess if the MaB presence affects Re photoelectrons energies.

Data collection began with survey scans of each sample (Fig. S1–S11, SI). XPS survey spectra revealed the following elements: Re, O, N, C (in one case some amounts of adsorbed Ag on the surface of crystals was also observed – Fig. S1). Various photoelectron signals were detected for rhenium in the survey spectra of perrhenate salts **1** and **2**, including Re 4f, Re 4d, and Re 4p emissions. The ensuing discussion will only focus on the Re 4f photoelectron energies due to their higher intensity and closer proximity in energy to the rhenium valence shell, making it particularly responsive to slight alterations in the chemical state of rhenium and the interaction pattern it is involved in.

A brief literature survey was performed in order to gain a better understanding of trends for Re 4f energies in XPS spectra of Re^{7+} derivatives. This survey revealed considerable differences in the reported $4f_{7/2}$ BEs that can vary in the range 45.2–46.9 eV.[57–59] For instance, these energies are 45.3 and 46.3 eV for the relatively similar salts $AgReO_4$ and NH_4ReO_4.[59–61] However, the majority of Re $4f_{7/2}$ energy values for Re^{7+} structures are greater than 46.0 eV (ref. 59, 60 and 62–65) and the deviation from $Re^{7+} \geq 46.0$ eV may be related to the presence of non-covalent interactions which redistributes the electron density around Re.

Subsequently, high-resolution XPS spectra were acquired for perrhenate salts **1a–h** and **2a–c** (Fig. 3 and S1–11). BEs values for Re $4f_{7/2}$ are lower than 46.0 eV in matere bonded salts **1a–h** while are higher than 46.0 eV (consistent with the majority of literature data) in salts **2a–c** wherein no MaB is present. For example, the BE of the Re $4f_{7/2}$ signal in **1b** and **1f** is 0.8 or 1.2 eV at lower energies than in **2a** and in **1d** it is approximately at 0.5 eV at lower energies than in **2b** or **2c** (Table 2). Typical XPS BEs uncertainties are ~0.1 eV, so the observed BEs changes cannot be ascribed primarily to measurement uncertainties[66] and it can be dependably stated that the Re $4f_{7/2}$ signals of

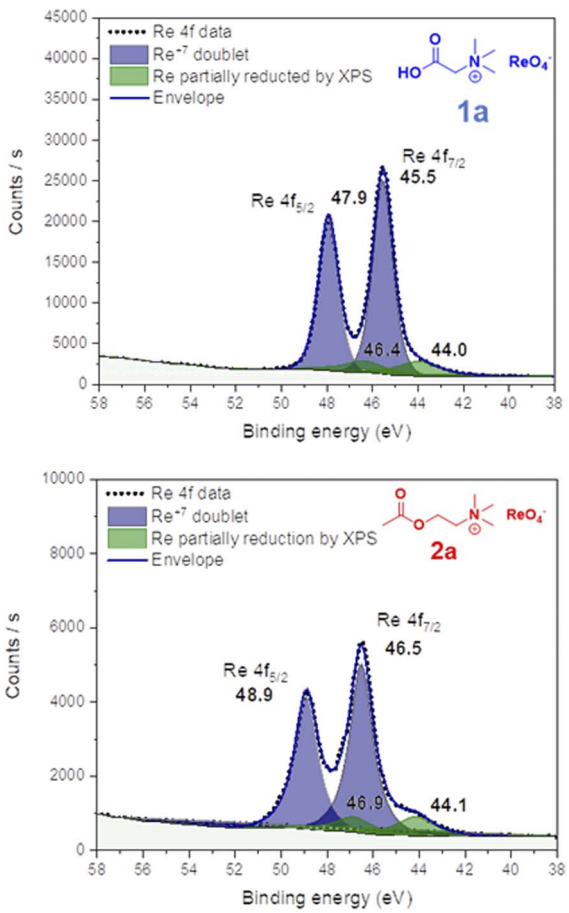

Fig. 3 Re 4f processed spectra of compounds **1a** and **2a**. Table 2. X-ray and XPS data of perrhenate salts **1a–h** and **2a–c**.

Table 2 X-ray and XPS data of perrhenate salts **1a–h** and **2a–c**

Perrhenate salt	MaB Nc	MaB length (Å)	XPS Re $4f_{7/2}$[a] (eV)
1a	0.925	3.329	45.5
1b	0.959	3.454	45.7
1c	0.956	3.441	45.7
1d	0.957	3.445	45.7
1e	0.942	3.392	45.7
1f	0.880	3.168	45.3
1g	1.03	3.717	45.8–45.9
1h	0.85	3.052	45.2–45.3
2a	—	—	46.5
2b	—	—	46.1
2c	—	—	46.1

[a] The instrumental binding-energy accuracy is ±0.1 eV.

perrhenate salts are at lower binding energies when MaB is present and at higher energies when this interaction is absent.

The BE shift to lower energies induced by MaB is consistent with the nature of the interaction. The Re $4f_{7/2}$ BE increases with the oxidation state of rhenium, specifically it is 40.5, 43.0, 45.4, and 46.7 eV in elemental rhenium, ReO_2, ReO_3, and Re_2O_7, respectively.[67] On Re···O MaB formation, donation of electron density occurs from an oxygen lone pair to a rhenium antibonding orbital (see onwards) and the increased electron density at rhenium translates into a lower Re $4f_{7/2}$ binding energy (Fig. S12).

Moreover, there is a correlation ($r = 0.91$) between the Re $4f_{7/2}$ photoelectron BE and the MaB length, specifically the former decreases with the latter (Fig. 4). Ordinary least squares regression of the experimental data (compounds **1a–1h**) gives $BE = (1.00 \pm 0.13) \times d(Re\cdots O) + (42.21 \pm 0.44)$ eV, $R^2 = 0.906$ ($r \approx 0.95$, $p = 2.7 \times 10^{-4}$, $n = 8$). The 95% confidence intervals are 0.68–1.32 eV $Å^{-1}$ for the slope and 41.12–43.30 eV for the intercept. The residual standard error (0.070 eV) is in line with the ±0.1 eV experimental accuracy, confirming that the observed correlation is statistically significant. Compound **1f** shows the shortest MaB bond among the hybrid organic–inorganic salts and the smallest Re BE, the inorganic salt $AgReO_4$ (**1h**) has an even shorter MaB bond length[68] and it seem to have a smaller Re BE than **1f** (Table 2). This correlation between

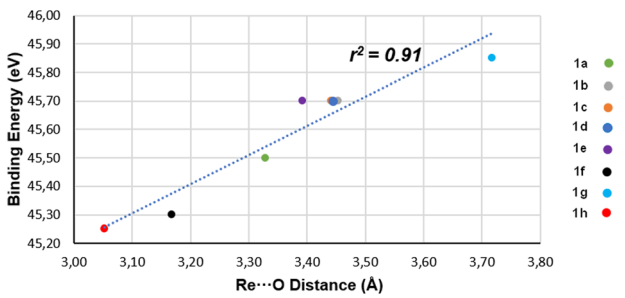

Fig. 4 Correlation between Re $4f_{7/2}$ BE from XPS analysis (the values 45.85, and 45.25 have been used for **1g**, and **1h**) and Re···O distance from single-crystal XRD.

binding energies and MaB separation is consistent with the MaB nature. It is well established that the charge-transfer component of σ-hole interactions increases when the interaction length decreases. In shorter Re···O contacts the electron density donation from oxygen to rhenium is greater and the increased electron density on Re translates into lower Re $4f_{7/2}$ BEs.

Various structural features, such as hydrogen bonding networks and counterion effects, could potentially influence the observed Re $4f_{7/2}$ binding energies, but these interactions primarily involve the perrhenate anion's oxygen atoms and do not directly engage the rhenium atom. Consequently, their influence on the Re $4f_{7/2}$ binding energy is likely to be minimal. Furthermore, the robust correlation observed between the matere bond length and the Re $4f_{7/2}$ BE (Fig. 4) provides compelling evidence for the dependence of the former parameter on the second one, largely independent of other ancillary interactions.

To obtain further information on the correlation between XPS and MaB length, we utilized Density Functional Theory (DFT) calculations with a focus on Natural Bond Orbital (NBO) analysis. This technique is especially suitable for comparing MaBs unaffected by intense electrostatic interactions. For example, the interaction in compound **1a** involves counterions, whereas in other compounds it is an anion···anion interaction.

Importantly, the LP(O) → σ*(Re–O) charge-transfer is closely related to the interacting distance (orbital overlap), which correlates with the binding energy, as demonstrated below. Table 3 presents the NBO second-order perturbation energies [$E^{(2)}$] for the compounds examined in this theoretical study, corresponding solely to the LP(O) → σ*(Re–O) donor–acceptor interaction. Fig. 5a–c illustrates the three distinct binding modes identified in these compounds, along with the specific NBOs involved in the MaBs. In every system, the characteristic LP(O) → σ*(Re–O) charge transfer was noted. Specifically, in the anion antiparallel dimer observed in **1d,e** featuring two symmetric LP(O) → σ*(Re–O) electron donations, only half of the total second-order stabilization energy ($E^{(2)}$) value is listed in Table 3. This represents the contribution of one MaB, allowing for direct comparison with the other complexes.

An analysis of Table 3 shows that compound **1g**, characterized by the longest MaB distance and the lowest binding energy, also has the lowest $E^{(2)}$ value. Conversely, compound **1f**, with the shortest MaB distance, exhibits the highest experimental binding energy and NBO $E^{(2)}$ energies. Notably, a good correlation ($r = 0.9511$) has been identified between the experimental binding energy and the theoretical second-order stabilization energy, as depicted in Fig. 5d. This finding implies that the variation in XPS values experimentally observed is associated

Table 3 Second-order stabilization energies ($E^{(2)}$) calculated in this study

Compound	**1a**	**1b**	**1c**	**1d**	**1e**	**1f**	**1g**
$E^{(2)}$ (kJ mol^{-1})	2.1	0.8	1.0	1.5	1.8	4.5	0.2

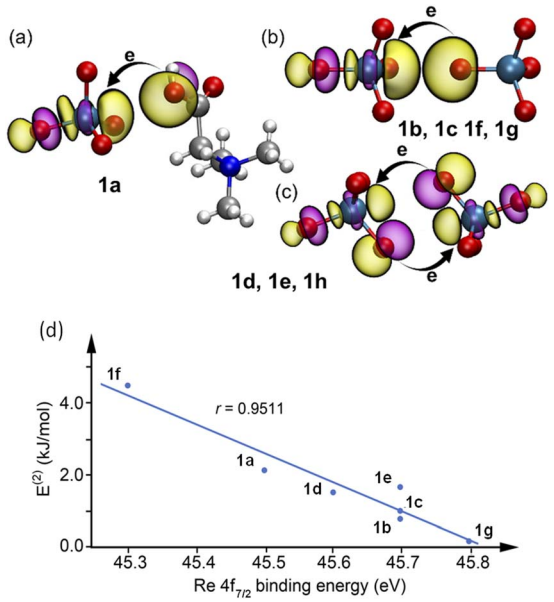

Fig. 5 Plots of the NBOs involved in the three types of MaB observed in compounds **1a** (a), **1b,c,f,g** (b) and **1d,e,h** (c). Regression plot (d) of the NBO stabilization energies $E^{(2)}$ and the Re $4f_{7/2}$ BEs derived from XPS the value 45.8 have been used for **1g**.

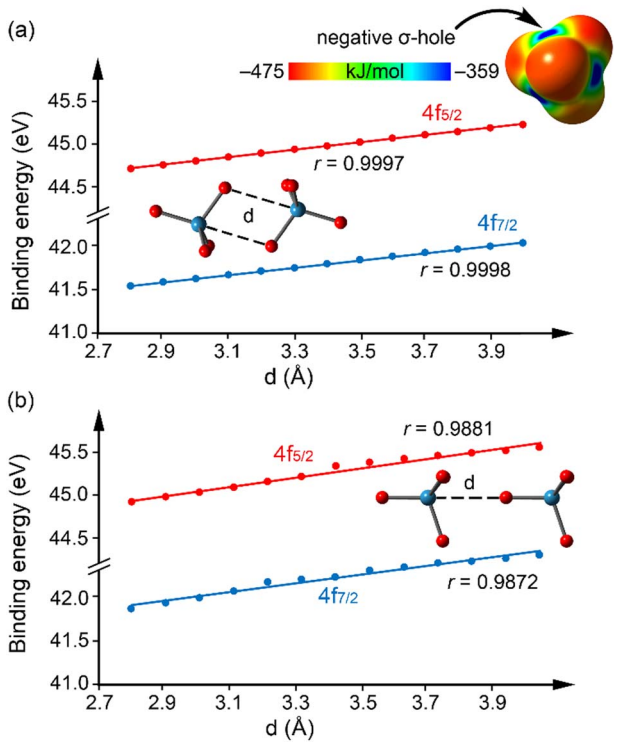

Fig. 6 The molecular electrostatic potential (MEP) surface is shown in the upper part of the figure, with a MEP value of −359 kJ mol^{-1} at the rhenium σ-holes and −475 kJ mol^{-1} at the oxygen atoms. The lower part displays correlation plots (a and b) between the theoretical Re 4f BEs and the corresponding Re···O distances.

with the formation of the MaB. The significance of this correlation, particularly evident in the regression plot, underscores the role of electron charge transfer to the rhenium σ-hole. This transfer leads to a redistribution of electron density around the Re-atoms, thereby facilitating the release of a 4f electron from the Re atom.

To further investigate the direct relationship between MaB separation and the Re 4f BE, we computed the theoretical XPS spectrum of an isolated perrhenate molecule and examined how this spectrum changes upon formation of both linear and antiparallel homodimers. In addition, we evaluated how BE values vary as a function of the Re···O distance, ranging from 2.8 to 4.0 Å. As shown by the NBO analysis (Fig. 5d), charge transfer from the oxygen atom to the σ-hole on rhenium increases with decreasing interaction distance, leading to lower Re 4f BEs. This trend is further supported by theoretical simulations (Fig. S13, SI), which compare the spectra of monomers and dimers at various distances. Notably, we observed strong correlations (Fig. 6) between the MaB distance and the BEs of both the $4f_{7/2}$ and $4f_{5/2}$ bands. These results provide strong theoretical support for the experimental findings and effectively rule out alternative explanations – such as counterion effects or crystal packing – as the source of the observed changes in the XPS spectra.

Conclusions

In this paper we prove that XPS is a suitable spectroscopic technique to detect the matere bond (MaB) presence involving the rhenium atom of perrhenate anions as the electrophilic atom. The interaction presence correlates with negative shifting (about 0.3–1.2 eV) in the binding energy of Re $4f_{7/2}$ and it thus become possible to differentiate between salts wherein MaB driven anion···anion self-assembly occurs from those wherein it does not. The XPS technique complements the single crystal X-ray analyses for assessing the MaB presence. It offers the advantage of working on non-crystalline, or microcrystalline, solids and of requiring relatively short measurement time so that it is amenable for routine analyses.

A strong correlation was established between the Re···O distance and the Re 4f binding energy, as both experimental and theoretical XPS analyses confirm that shorter MaBs are associated with lower Re 4f binding energies. This effect originates from increased electron density donation from the oxygen atom to the rhenium σ-hole, as verified by Natural Bond Orbital (NBO) analyses and second-order perturbation energy calculations. Theoretical modeling of isolated perrhenate monomers and dimers further supports these findings, ruling out alternative influences such as counterions or packing effects.

Together, these experimental and theoretical insights confirm that XPS not only identifies the presence of MaBs but also provides meaningful information about their geometric and electronic characteristics, establishing it as a robust tool for studying σ-hole interactions in non-crystalline materials.

Experimental

Materials

All compounds were purchased from commercial suppliers (Merck, abcr) and used without further purification.

General synthetic procedure of salts 1a–g, 2a–c

0.5 mmol of base are dissolved in 5 mL of a 0.1 M aqueous solution of HCl. 0.5 mmol of $AgReO_4$ are then added to the solution. A whitish solid precipitates immediately. After 5 hours, the solution is filtered and the liquid is left to slowly evaporate in a clear borosilicate vial at room temperature. Colorless crystals suitable for single crystal X-ray diffraction form within one week. The same procedure was scaled up for preparing salt amounts suitable for XPS analysis.

X-ray data collection

The single crystal data of the compounds were collected at room temperature using a Bruker SMART APEX II CCD area detector diffractometer. Data collection, unit cell refinement and data reduction were performed using Bruker SAINT. Structures were solved by direct methods using SHELXT[69] and refined by full-matrix least-squares on F^2 with anisotropic displacement parameters for the non-H atoms using SHELXL-2016/6.[70] Absorption correction was performed based on multi-scan procedure using SADABS. Structure analysis was aided by use of the programs PLATON.[71] The hydrogen atoms were calculated in ideal positions with isotropic displacement parameters set to $1.2 \times U_{eq}$ of the attached atom.

Computational methods

The NBO analyses were computed as single point calculations taking the geometries of the studied units from the crystal structures at the RI-PBE0 (ref. 72)-D4 (ref. 73)//def2-TZVP[74] level of theory, using the NBO7.0 (ref. 75) software integrated in the Gaussian 16 (ref. 76) software package. To gather insights on the theoretical XPS spectra, we performed calculations at the ZORA[77]-PBE0-D4//ma-def2-TZVP[78] (SARC-ZORA-TZVP,[79] for the Re atoms) level of theory as to compute and obtain a wavefunction which accounted for the relativistic effects of the heavier Re atoms and described its more inner electrons using the ORCA[80] software package. The obtained wavefunction was then treated using the Multiwfn[81] software to obtain the XPS spectra. The models used in this case to study the variations in the XPS spectra, were obtained from two separated optimized perrhenate anions which were then oriented as to have a O⋯Re–O angle of 180° and then their XPS spectra were plotted at selected O⋯Re distances (see Fig. 6). This was done for two different sets: one displaying a single MaB interaction (Fig. 6b) and another displaying a double MaB where both units act as MaB donor and acceptor (Fig. 6a). The Molecular Electrostatic Potential surfaces (MEP) were obtained as well from the computed wavefunction, making use of the Multiwfn program.

XPS measurements

For XPS study, an appropriate single crystal was collected from the crystalized powder. Every crystallization batch has been additionally studied using single crystal X-ray diffraction in order to prove the structure. The chosen crystals of compounds **1a–h**, **2a–c**, were deposited onto copper conductive tape and gently pressed with a spatula. Measurements were performed on a Thermo Fisher Scientific NEXSA XPS spectrometer equipped with a monochromated Al Kα X-ray source (1486.6 eV). The analyzed area was 100–400 μm^2, and charge compensation was provided by a flood gun. X-Ray was focused directly on the surface of single crystal. Survey spectra were recorded at a pass energy of 200 eV with an energy resolution of 1 eV. The high-resolution spectra (C 1s, N 1s, O 1s, Ag 3d, Re 4f) were acquired at a pass energy of 50 eV with an energy resolution of 0.1 eV. No charge compensation nor argon etching nor binding energy correction by setting the C(1s) were applied. The accuracy of high-resolution XPS measurements is ±0.1 eV, corresponding to the instrumental resolution of the NEXSA spectrometer. Multiple measurements for each compound showed smaller variability, confirming that deviations below this value are not meaningful.

Author contributions

O. S. and O. G., performed XPS analyses and prepared a draft of the manuscript; N. S. A., A. D. R., A. P., and C. L. prepared the compounds, performed X-ray analyses, and prepared a draft of the manuscript; S. B. and A. F. performed the theoretical analyses, and prepared a draft of the manuscript; G. R., P. S. P., A. F., and A. P. designed the research and prepared the final draft of the manuscript.

Conflicts of interest

There are no conflicts to declare.

Data availability

CCDC 2442760 (for **1d**), 2442761 (for **1e**), 2442763 (for **1f**), 2442772 (for **1g**) and 2442773 (for **2b**) contain the supplementary crystallographic data for this paper.[82a–e]

The authors confirm that the data supporting the findings of this study are available within the article and SI file. See DOI: **https://doi.org/10.1039/d5sc04587h**.

Acknowledgements

Support from the Ministry of Science and Higher Education of the Russian Federation in the framework of the "Mega-grant" project (No. 075-15-2021-585s) and GACR (GACR No. 22-02022S) is gratefully acknowledged. The authors also thank the central laboratories of TPU (Analytical center) for the XPS measurements. AF and AB are grateful to Project PID2023-148453NB-I00 funded by the Ministerio de Ciencia, Innovación y Universidades of Spain MCIU/AEI/10.13039/501100011033 and FEDER, UE.

Notes and references

1 P. Politzer, J. S. Murray, T. Clark and G. Resnati, *Phys. Chem. Chem. Phys.*, 2017, **19**, 32166–32178.
2 G. Cavallo, P. Metrangolo, T. Pilati, G. Resnati and G. Terraneo, *Cryst. Growth Des.*, 2014, **14**, 2697–2702.

3 P. S. Ho, *Future Med. Chem.*, 2017, **9**, 637–640.
4 R. L. Sutar and S. M. Huber, *ACS Catal.*, 2019, **9**, 9622–9639.
5 S. Benz, J. López-Andarias, J. Mareda, N. Sakai and S. Matile, *Angew. Chem., Int. Ed.*, 2017, **56**, 812–815.
6 A. Mukherjee, S. Tothadi and G. R. Desiraju, *Acc. Chem. Res.*, 2014, **47**, 2514–2524.
7 P. Scilabra, G. Terraneo and G. Resnati, *Acc. Chem. Res.*, 2019, **52**, 1313–1324.
8 J. Y. C. Lim and P. D. Beer, *Chem*, 2018, **4**, 731–783.
9 A. Bertolani, L. Pirrie, N. Houbenov, J. Haataja, L. Stefan, L. Catalano, G. Terraneo, G. Giancane, L. Valli, R. Milani, O. Ikkala, G. Resnati and P. Metrangolo, *Nat. Commun.*, 2015, **6**, 1–9.
10 G. Cavallo, P. Metrangolo, R. Milani, T. Pilati, A. Priimagi, G. Resnati and G. Terraneo, *Chem. Rev.*, 2016, **116**, 2478–2601.
11 G. R. Desiraju, P. S. Ho, L. Kloo, A. C. Legon, R. Marquardt, P. Metrangolo, P. Politzer, G. Resnati and K. Rissanen, *Pure Appl. Chem.*, 2013, **85**, 1711–1713.
12 M. C. Ford and P. S. Ho, *J. Med. Chem.*, 2016, **59**, 1655–1670.
13 S. Jiang, L. Zhang, D. Cui, Z. Yao, B. Gao, J. Lin and D. Wei, *Sci. Rep.*, 2016, **6**, 34750.
14 L. Mendez, G. Henriquez, S. Sirimulla and M. Narayan, *Molecules*, 2017, **22**, 1397.
15 G. Berger, P. Frangville and F. Meyer, *Chem. Commun.*, 2020, **56**, 4970–4981.
16 Y. Chan and Y. Yeung, *Angew. Chem., Int. Ed.*, 2018, **57**, 3483–3487.
17 S. Benz, A. I. Poblador-Bahamonde, N. Low-Ders and S. Matile, *Angew. Chem., Int. Ed.*, 2018, **130**, 5506–5510.
18 R. Gulyaev, O. Semyonov, G. V. Mamontov, A. A. Ivanov, D. M. Ivanov, M. Kim, V. Švorčík, G. Resnati, T. Liao, Z. Sun, Y. Yamauchi, P. S. Postnikov and O. Guselnikova, *ACS Mater. Lett.*, 2023, **5**, 1340–1349.
19 X. Fu, T. He, S. Zhang, X. Lei, Y. Jiang, D. Wang, P. Sun, D. Zhao, H.-Y. Hsu, X. Li, M. Wang and M. Yuan, *Chem*, 2021, **7**, 3131–3143.
20 P. Metrangolo, L. Canil, A. Abate, G. Terraneo and G. Cavallo, *Angew. Chem., Int. Ed.*, 2022, **61**, e202114793.
21 M. L. Ball, J. V. Milić and Y.-L. Loo, *Chem. Mater.*, 2022, **34**, 2495–2502.
22 C. B. Aakeroy, D. L. Bryce, G. R. Desiraju, A. Frontera, A. C. Legon, F. Nicotra, K. Rissanen, S. Scheiner, G. Terraneo, P. Metrangolo and G. Resnati, *Pure Appl. Chem.*, 2019, **91**, 1889–1892.
23 G. Resnati, D. L. Bryce, G. R. Desiraju, A. Frontera, I. Krossing, A. C. Legon, P. Metrangolo, F. Nicotra, K. Rissanen, S. Scheiner and G. Terraneo, *Pure Appl. Chem.*, 2024, **96**, 135–145.
24 S. Scheiner, *Phys. Chem. Chem. Phys.*, 2021, **23**, 5702–5717.
25 A. Daolio, M. Calabrese, A. Pizzi, C. Lo Iacono, N. Demitri, R. Beccaria, R. M. Gomila, A. Frontera and G. Resnati, *Chem.–Eur. J.*, 2024, **30**, 1–8.
26 A. Daolio, P. Scilabra, G. Terraneo and G. Resnati, *Coord. Chem. Rev.*, 2020, **413**, 213265.
27 S. J. Grabowski, *Coord. Chem. Rev.*, 2020, **407**, 213171.
28 A. Pizzi, G. Terraneo, C. Lo Iacono, R. Beccaria, A. Dhaka and G. Resnati, *Angew. Chem., Int. Ed.*, 2025, **64**, e202506525.
29 G. Resnati and P. Metrangolo, *Coord. Chem. Rev.*, 2020, **420**, 213409.
30 A. Daolio, A. Pizzi, M. Calabrese, G. Terraneo, S. Bordignon, A. Frontera and G. Resnati, *Angew. Chem., Int. Ed.*, 2021, **133**, 20891–20895.
31 A. Daolio, A. Pizzi, G. Terraneo, M. Ursini, A. Frontera and G. Resnati, *Angew. Chem., Int. Ed.*, 2021, **133**, 14506–14510.
32 A. Daolio, A. Pizzi, M. Calabrese, N. Demitri, J. S. Murray, P. Politzer and G. Resnati, *Cryst. Growth Des.*, 2023, **23**, 574–579.
33 M. Calabrese, R. M. Gomila, A. Pizzi, A. Frontera and G. Resnati, *Chem.–Eur. J.*, 2023, **29**, 1–6.
34 J. Halldin Stenlid, A. J. Johansson and T. Brinck, *Phys. Chem. Chem. Phys.*, 2018, **20**, 2676–2692.
35 A. Bauzá, I. Alkorta, J. Elguero, T. J. Mooibroek and A. Frontera, *Angew. Chem., Int. Ed.*, 2020, **59**, 17482–17487.
36 M. Michalczyk, W. Zierkiewicz and S. Scheiner, *Phys. Chem. Chem. Phys.*, 2024, **26**, 5836–5847.
37 C. Lo Iacono, A. Pizzi, K. T. Mahmudov, R. M. Gomila, A. Frontera and G. Resnati, *Cryst. Growth Des.*, 2025, **25**, 4338–4347.
38 A. Daolio, A. Pizzi, G. Terraneo, A. Frontera, G. Resnati, A. Daolio, A. Pizzi, G. Terraneo, G. Resnati and A. Frontera, *ChemPhysChem*, 2021, **22**, 2281–2285.
39 M. Calabrese, A. Pizzi, A. Daolio, A. Frontera and G. Resnati, *Dalton Trans.*, 2023, **52**, 1030–1035.
40 A. Pizzi, A. Dhaka, R. Beccaria and G. Resnati, *Chem. Soc. Rev.*, 2024, **53**, 6654–6674.
41 A. Frontera and A. Bauzá, *Chem.–Eur. J.*, 2018, **24**, 7228–7234.
42 M. de las, N. Piña, A. Frontera and A. Bauzá, *J. Phys. Chem. Lett.*, 2020, **11**, 8259–8263.
43 A. Terrón, J. Buils, T. J. Mooibroek, M. Barceló-Oliver, A. García-Raso, J. J. Fiol and A. Frontera, *Chem. Commun.*, 2020, **56**, 3524–3527.
44 M. Calabrese, A. Pizzi, A. Daolio, R. Beccaria, C. Lo Iacono, S. Scheiner and G. Resnati, *Chem.–Eur. J.*, 2024, **30**, e202304240.
45 J. L. Bourque, M. C. Biesinger and K. M. Baines, *Dalton Trans.*, 2016, **45**, 7678–7696.
46 M. Fantauzzi, B. Elsener, D. Atzei, A. Rigoldi and A. Rossi, *RSC Adv.*, 2015, **5**, 75953–75963.
47 J. S. Stevens, L. K. Newton, C. Jaye, C. A. Muryn, D. A. Fischer and S. L. M. Schroeder, *Cryst. Growth Des.*, 2015, **15**, 1776–1783.
48 J. S. Stevens, S. J. Byard, C. C. Seaton, G. Sadiq, R. J. Davey and S. L. M. Schroeder, *Phys. Chem. Chem. Phys.*, 2014, **16**, 1150–1160.
49 J. S. Stevens, S. Coultas, C. Jaye, D. A. Fischer and S. L. M. Schroeder, *Phys. Chem. Chem. Phys.*, 2020, **22**, 4916–4923.
50 S. Tothadi, T. R. Shaikh, S. Gupta, R. Dandela, C. P. Vinod and A. K. Nangia, *Cryst. Growth Des.*, 2021, **21**, 735–747.
51 Q. Zhao, S. Lin, P. Sun, Y. Lu, Q. Li, Z. Tian, X. Bai, J. Wang, L. Wang and S. Chen, *Adv. Funct. Mater.*, 2025, **2421755**, 1–9.

52 Y. Xu, M. Calabrese, N. Demitri, A. Pizzi, T. Nag, I. Hung, Z. Gan, G. Resnati and D. L. Bryce, *Chem. Commun.*, 2023, **59**, 12609–12612.
53 R. Beccaria, A. Pizzi, G. Resnati and D. L. Bryce, *ChemPhysChem*, 2025, e202401030.
54 R. Tepper, S. Bode, R. Geitner, M. Jäger, H. Görls, J. Vitz, B. Dietzek, M. Schmitt, J. Popp, M. D. Hager and U. S. Schubert, *Angew. Chem., Int. Ed.*, 2017, **56**, 4047–4051.
55 M. Calabrese, A. Pizzi, A. Daolio, A. Frontera and G. Resnati, *Chem. Commun.*, 2022, **58**, 9274–9277.
56 P. Czarnecki and H. Maluszynska, *J. Phys.: Condens. Matter*, 2000, **12**, 4881–4892.
57 J. Okal, W. Tylus and L. Kepinski, *J. Catal.*, 2004, **225**, 498–509.
58 M. T. Greiner, T. C. R. Rocha, B. Johnson, A. Klyushin, A. Knop-Gericke and R. Schlögl, *Z. Phys. Chem.*, 2014, **228**, 521–541.
59 E. S. Shpiro, V. I. Avaev, G. V. Antoshin, M. A. Ryashentseva and K. M. Minachev, *J. Catal.*, 1978, **55**, 402–406.
60 S. Iqbal, M. L. Shozi and D. J. Morgan, *Surf. Interface Anal.*, 2017, **49**, 223–226.
61 J. Wang, T. Li, T. Yan, X. Wei, X. Qu and S. Yuan, *Materials*, 2019, **12**, 2199.
62 S. Oktay, Z. Kahraman, M. Urgen and K. Kazmanli, *Appl. Surf. Sci.*, 2015, **328**, 255–261.
63 N. B. Egorov and E. A. Isaeva, *Inorg. Mater.*, 2022, **58**, 899–905.
64 J. Tang, Y. Sun, C. Zhang, L. Wang, Y. Zhou, D. Fang and Y. Liu, *Metals*, 2020, **10**, 640.
65 A. Cimino, B. A. De Angelis, D. Gazzoli and M. Valigi, *J. Inorg. Gen. Chem.*, 1980, **471**, 208–226.
66 K. N. Wood and G. Teeter, *ACS Appl. Energy Mater.*, 2018, **1**, 4493–4504.
67 **http://www.xpsfitting.com/2020/05/rhenium.html**.
68 D. Y. Naumov, A. V. Virovets, S. V. Korenev and A. I. Gubanov, *Acta Crystallogr., Sect. C: Cryst. Struct. Commun.*, 1999, **55**, IUC9900097.
69 G. M. Sheldrick, *Acta Crystallogr., Sect. A: Found. Crystallogr.*, 2015, **71**, 3–8.
70 G. M. Sheldrick, *Acta Crystallogr., Sect. C: Cryst. Struct. Commun.*, 2015, **71**, 3–8.
71 A. L. Spek, *Acta Crystallogr., Sect. D: Biol. Crystallogr.*, 2009, **65**, 148–155.
72 C. Adamo and V. Barone, *J. Chem. Phys.*, 1999, **110**, 6158–6170.
73 E. Caldeweyher, S. Ehlert, A. Hansen, H. Neugebauer, S. Spicher, C. Bannwarth and S. Grimme, *J. Chem. Phys.*, 2019, **150**, 154122.
74 F. Weigend, *Phys. Chem. Chem. Phys.*, 2006, **8**, 1057–1065.
75 E. D. Glendening, J. K. Badenhoop, A. E. Reed, J. A. Carpenter, J. E. Bohmann, C. M. Morales, P. Karafiloglou, C. R. Landis and F. Weinhold, *NBO 7.0*, Theor. Chem. Institute, Univ. Wisconsin, 2018.
76 M. J. Frisch, G. W. Trucks, H. B. Schlegel, G. E. Scuseria, M. A. Robb, J. R. Cheeseman, G. Scalmani, V. Barone, G. A. Petersson, H. Nakatsuji, X. Li, M. Caricato, A. Marenich, J. Bloino, B. G. Janesko, R. Gomperts, B. Mennucci, H. P. Hratchian, J. V. Ortiz, A. F. Izmaylov, J. L. Sonnenberg, D. Williams-Young, F. Ding, F. Lipparini, F. Egidi, J. Goings, B. Peng, A. Petrone, T. Henderson, D. Ranasinghe, V. G. Zakrzewski, J. Gao, N. Rega, G. Zheng, W. Liang, M. Hada, M. Ehara, K. Toyota, R. Fukuda, J. Hasegawa, M. Ishida, T. Nakajima, Y. Honda, O. Kitao, H. Nakai, T. Vreven, K. Throssell, J. A. J. Montgomery, J. E. Peralta, F. Ogliaro, M. Bearpark, J. J. Heyd, E. Brothers, K. N. Kudin, V. N. Staroverov, T. Keith, R. Kobayashi, J. Normand, K. Raghavachari, A. Rendell, J. C. Burant, S. S. Iyengar, J. Tomasi, M. Cossi, J. M. Millam, M. Klene, C. Adamo, R. Cammi, J. W. Ochterski, R. L. Martin, K. Morokuma, O. Farkas, J. B. Foresman and D. J. Fox, *Gaussian 19*, Gaussian, Inc., Wallingford CT, 2016.
77 E. Van Lenthe, J. G. Snijders and E. J. Baerends, *J. Chem. Phys.*, 1996, **105**, 6505–6516.
78 J. Zheng, X. Xu and D. G. Truhlar, *Theor. Chem. Acc.*, 2011, **128**, 295–305.
79 D. A. Pantazis, X. Y. Chen, C. R. Landis and F. Neese, *J. Chem. Theory Comput.*, 2008, **4**, 908–919.
80 F. Neese, *Wiley Interdiscip. Rev.: Comput. Mol. Sci.*, 2012, **2**, 73–78.
81 T. Lu and F. Chen, *J. Comput. Chem.*, 2012, **33**, 580–592.
82 (*a*) O. Semyonov, N. S. Antonkin, A. D. Radzhabov, A. Pizzi, C. Lo Iacono O. Guselnikova, S. Burguera, A. Frontera, G. Resnati and P. S. Postnikov, CCDC 2442760: Experimental Crystal Structure Determination, 2025, DOI: **10.5517/ccdc.csd.cc2mzwq7**.; (*b*) O. Semyonov, N. S. Antonkin, A. D. Radzhabov, A. Pizzi, C. Lo Iacono O. Guselnikova, S. Burguera, A. Frontera, G. Resnati and P. S. Postnikov, CCDC 2442761: Experimental Crystal Structure Determination, 2025, DOI: **10.5517/ccdc.csd.cc2mzwr8**; (*c*) O. Semyonov, N. S. Antonkin, A. D. Radzhabov, A. Pizzi, C. Lo Iacono O. Guselnikova, S. Burguera, A. Frontera, G. Resnati and P. S. Postnikov, CCDC 2442763: Experimental Crystal Structure Determination, 2025, DOI: **10.5517/ccdc.csd.cc2mzwtb**; (*d*) O. Semyonov, N. S. Antonkin, A. D. Radzhabov, A. Pizzi, C. Lo Iacono O. Guselnikova, S. Burguera, A. Frontera, G. Resnati and P. S. Postnikov, CCDC 2442772: Experimental Crystal Structure Determination, 2025, DOI: **10.5517/ccdc.csd.cc2mzx3n**; (*e*) O. Semyonov, N. S. Antonkin, A. D. Radzhabov, A. Pizzi, C. Lo Iacono O. Guselnikova, S. Burguera, A. Frontera, G. Resnati and P. S. Postnikov, CCDC 2442773: Experimental Crystal Structure Determination, 2025, DOI: **10.5517/ccdc.csd.cc2mzx4p**.